Research Square

Preprints are preliminary reports that have not undergone peer review.
They should not be considered conclusive, used to inform clinical practice,
or referenced by the media as validated information.

An Integrated Thermodynamic and Microphysical Framework for Thunderstorm and Lightning Prediction Using the WRF Model

Jannatul Ferdous Jerin
University of Dhaka
Pappu Paul
pappu.paul@du.ac.bd
University of Dhaka

Research Article

Keywords:

Posted Date: August 19th, 2026

DOI: https://doi.org/10.21203/rs.3.rs-10320358/v1

License: This work is licensed under a Creative Commons Attribution 4.0 International License.
Read Full License

Additional Declarations: No competing interests reported.

An Integrated Thermodynamic and Microphysical Framework for Thunderstorm and Lightning Prediction Using the WRF Model

Jannatul Ferdous Jerin[1] and Pappu Paul*[1,2]

[1]Department of Meteorology, University of Dhaka, Bangladesh
[2]Department of Climate, Meteorology & Atmospheric Sciences, University of Illinois Urbana Champaign, USA

Abstract

Bangladesh is located within the highly lightning-prone region (30N-30S belt) and experiences significant casualties and property loss, particularly during the pre-monsoon and monsoon season due to lightning activity. Traditional thunderstorm and lightning forecasting methods are mostly rely on thermodynamic instability indices. These indices have limitations in forecasting the intensity, duration, and spatial distribution of the lightning. Recent advances in high-resolution Numerical Weather Prediction (NWP) have facilitated the development of microphysics and cloud electrification-based techniques, such as the Lightning Potential Index (LPI) and Lightning Flash Density (LFD). They improve lightning forecasts with greater spatial accuracy but have a very shorter lead time. This study investigates four severe thunderstorm events occurring between May and July 2023 over Bangladesh using Weather Research and Forecasting (WRF) model with electrification scheme (WRF-Elec). Here, we investigate an integrated approach of thermodynamic and microphysical framework to improve lightning forecasting in both temporal and spatial dimensions. We find that microphysical fields like maximum reflectivity, LPI, and LFD capture the lightning activity with 2-6 hours lead time and spatial accuracy of 1.5×1.5 deg boundary. On the other hand, the conventional thermodynamic fields predict convective activity 10-12 hours lead time but provide the information of little to no spatial boundary. In the integrated approach combining microphysical and thermodynamic fields we find the lightning prediction with a significantly larger lead time while maintaining spatial accuracy for lightning activity. These findings indicate that the integrated microphysical–thermodynamic framework could be adopted more broadly to enhance short-term lightning prediction in different regions and operational forecasting settings.

Keywords: Microphysics, Thermodynamics, LPI, LFD, WRF-Elec

1 Introduction

Lightning is a perilous natural phenomenon that poses significant risks to life, property, and socioeconomic stability, especially in vulnerable regions like Bangladesh. Bangladesh is situated within the 30°N–30°S latitudinal belt, where nearly 78% of global lightning strikes are concentrated (Christian et al., 2003). More lightning fatalities occur during the pre-monsoon season (March-May) and the monsoon season (June–September). From 2016, the Bangladesh government has started considering lightning strikes as a catastrophic weather event due to loss of life and property (Dewan et al., 2017). Unfortunately, the forecast of lightning in Bangladesh is not yet fully developed. Hence, a systematic and efficient lightning flash prediction and resilience is a necessity.

For this concern, meteorologists all over the world have typically rely on indices like Total-Totals Index (TTI), K index (KI), Convective Available Potential Energy (CAPE), Convective Inhibition (CIN) and other thermodynamic fields to forecast thunderstorm probabilities. Although these indices are widely used, they all have significant drawbacks. They primarily rely on thermodynamic probabilities and ignore important dynamical and microphysical processes that govern storm electrification, including charge separation mechanisms, ice-graupel interactions, and mesoscale convection organization (Lynn and Yair, 2010; Paul et al., 2019, 2022). This makes them effective at capturing the potential for thunderstorm initiation (Bondyopadhyay and Mohapatra, 2023) but less effective at predicting the intensity, duration, or lightning hazard associated with specific events(Kunz, 2007). Furthermore, in areas like Bangladesh that have complicated terrain or extremely variable boundary-layer conditions, their predictive accuracy is frequently limited by their coarse spatial and temporal resolution.

*Corresponding author: pappu.paul@du.ac.bd

Consequently, world forecasting community has moved toward microphysics based indices derived from NWP models that explicitly represent storm microphysics and electrification processes. Among these, the LPI has emerged as a promising diagnostic tool. Yair et al. (2010) and Lynn and Yair (2008) show that LPI is positively correlated with observed lightning density and also heavy rainfall, and suggest that LPI can be used to predict the potential for the occurrence of lightning. In recent times, the lightning prediction from numerical models has gathered a lot of interest because of its promising results (Vani K et al., 2022; Rabbani et al., 2022; Paul et al., 2022). Conventional techniques frequently rely on statistical relationships obtained from surface or upper-air observations and provide a broad prediction of the likelihood of thunderstorms. However, high-resolution NWP models that take environmental variability, dynamics, and microphysics into account, can simulate atmospheric processes. This approach improves the accuracy of identifying the lightning location (Ahasan et al., 2021; Ferdaus et al., 2021). However, the usefulness of LPI for prediction is limited, as it is typically available only when convection has already developed and the event is imminent. Consequently, LPI serves primarily as a nowcasting tool rather than a true forecasting indicator with meaningful lead time.

Another promising approach for predicting lightning activity in WRF is the explicit electrification and lightning parameterization framework, commonly referred to as WRF-Elec. This scheme is based on the electrification framework introduced by Mansell et al. (2005, 2010), which represents non-inductive charging, charge separation, electric-field development, and discharge processes within convective storms. The implementation of this explicit charging and discharge scheme in WRF-ARW is further developed by Fierro et al. (2013), enabling the simulation of storm electrification in different convective environments. Through this framework, WRF can provide lightning-related variables such as electric potential, electric-field magnitude, and lightning flash density, which are useful for short-term lightning prediction and hazard assessment.

Several studies demonstrate the usefulness of these approaches for regional lightning prediction. For example, the study of Gharaylou et al. (2019) compares LPI and WRF-ELEC-derived electric potential difference and finds that both diagnostics reproduce the observed lightning locations reasonably well. In a follow-up study, they show that WRF-ELEC lightning prediction is sensitive to initial and boundary conditions, with simulated LPI generally agreeing with World Wide Lightning Location Network (WWLLN) and LIS lightning observations Gharaylou et al. (2020). In another study, Mohan et al. (2021) evaluates several WRF lightning parameterization schemes and LPI for pre-monsoon lightning cases, while Vani K et al. (2022) further assesses the usefulness of WRF-based lightning forecasts for the Indian subcontinent. Srivastava et al. (2023) evaluates WRF-ELEC forecasts over northeast India and reports useful short-range skill, especially when lightning data assimilation is applied. More recently, Mahapatra et al. (2026) compares WRF-ELEC flash-origin density with LPI-derived lightning density over Odisha and finds that WRF-ELEC provides lower spatial and intensity mismatch than LPI.

Over Bangladesh, previous studies have examined either thermodynamic instability indices or WRF-based lightning diagnostics. Paul et al. (2019) shows that thermodynamic indices such as CAPE, CIN, TTI, and KI can indicate thunderstorm-favorable environments at relatively long lead times, but these indices provide limited information on the precise location of lightning activity. Similarly, Paul et al. (2022) assesses the Lightning Potential Index over Bangladesh and shows that LPI can represent thunderstorm occurrence and location, but its useful lead-time window remains relatively short. Rabbani et al. (2022) evaluates lightning forecasting using LPI and electric-potential-based approaches and shows that WRF-based lightning diagnostics can capture observed lightning activity with useful spatial guidance. More recently, Paramanik et al. (2024) examines diagnostic and explicit lightning parameterizations in WRF over Bangladesh and highlightes the importance of model physics choices, including microphysics and planetary boundary layer schemes, for lightning prediction.

While these studies highlight the capability of WRF-Elec and its associated lightning schemes to reproduce specific lightning events and evaluate parameterization performance, critical information regarding lead time is still lacking. In addition, no comprehensive assessment has evaluated the model's ability to predict lightning in Bangladesh using a coupled thermodynamic–microphysical framework capable of providing both extended lead times and improved spatial accuracy.

Addressing this issue requires an analysis of the coupled approach. To investigate this, we have design the present study as follows: Section 2 describes the datasets, model configuration, and experimental design. Section 3 presents the results and discussion, including an evaluation of key predictors and their relevance for lightning activity over Bangladesh. Finally, Section 4 summarizes the major findings, outlines the conclusions of this work and recommendations of future work.

2 Data & Methodology

2.1 WRF Model and Data

We use National Centers for Environmental Prediction (NCEP) Final (FNL) Operational Global Analysis data to run the WRF model in this study. The FNL dataset is produced operationally by NCEP using the Global Data Assimilation System (GDAS), which assimilates a wide range of in situ and satellite-based observations to generate gridded analyses of the atmospheric state.

The NCEP-FNL datasets are available every six hours (at 00, 06, 12, and 18 UTC) on a $1^\circ \times 1^\circ$ latitude–longitude grid, providing global coverage of essential meteorological variables such as temperature, pressure, humidity, wind components,

Table 1: WRF Model Configuration

Parameter	Configuration
DX, DY	4 km
Microphysics scheme	NSSL 2-moment (Mansell et al., 2010)
Electrification	ON(Ziegler and MacGorman, 1994)
Boundary layer scheme	Yonsei University scheme (YSU) (Hong et al., 2006)
Land surface model	Unified Noah Land Surface Model (Tewari, 2004)
Radiation	RRTMG (Iacono et al., 2008)

and surface fluxes. The FNL data are dynamically downscaled using the WRF model using the configuration in Table 1 to generate the high-resolution initial and boundary conditions required for simulating mesoscale convective systems and associated lightning activity over Bangladesh. The lateral boundary conditions are updated every six hours to maintain consistency with the evolving large-scale flow, while the model topography and land–surface fields are interpolated to the finer computational grid. The actual event time is positioned near the midpoint of the 24-hour simulation for each event to facilitate analysis of the pre-event and post-event atmospheric conditions and to ensure that any consecutive or evolving events are adequately captured. The model output interval is set to 10 minutes for all simulations.

The model physics schemes are selected based on their relevance to convective-scale lightning simulation and their use in previous WRF-based thunderstorm and lightning studies over Bangladesh. The NSSL 2-moment microphysics scheme is used because the WRF-Elec electrification module is built to operate with it, relying on the charge-separation framework established by Mansell et al. (2005, 2010) and later extended by Fierro et al. (2013) into an explicit charging and discharge scheme. In this configuration, both non-inductive and inductive charging are enabled, lightning discharge is activated, and the screening-layer scheme (Ziegler et al., 1991) is included. The WRF-Elec lightning scheme is selected because previous Bangladesh studies shows that explicit electrification-based simulations can reasonably reproduce observed lightning-prone regions and often perform better than purely diagnostic lightning methods (Rabbani et al., 2022; Paramanik et al., 2024). The YSU planetary boundary layer scheme is a widely used non-local PBL scheme with explicit entrainment treatment and is found to perform well in Bangladesh lightning sensitivity experiments when compared with MYNN and TEMF schemes Hong et al. (2006); Paramanik et al. (2024). The Noah land surface model and RRTMG radiation schemes are standard WRF schemes for representing land–atmosphere heat and moisture exchange and shortwave-longwave radiative fluxes, respectively Zhuo et al. (2019). The 4 km horizontal grid spacing (DX, DY) is selected because numerical weather and climate models at this resolution can begin to explicitly represent deep convective processes, thereby reducing reliance on deep-convection parameterization schemes that may introduce additional uncertainty (Prein et al., 2015). The LPI results are only significant in the convection resolving mode, i.e. The grid spacing of less than or equal to 4 km, and deep convection parameterization turned off Gofa et al. (2023). The finer the resolution the more resolved the small scale process than parametrization. However there is always a trade off between the computational cost and the accuracy. We find that 4 km grid size is optimal for the lightning prediction given that the computational constraints and also recent studies also verify this (Kain et al., 2008; Schwartz et al., 2009; Johnson et al., 2013)

Table 2: Summary of the selected lightning cases, including observed event date and time, representative 1.5×1.5° case coordinate, and corresponding WRF simulation start and end times (MM DD, UTC).

Case	Event Time	Coordinate (1.5×1.5 deg)	Simulation Start	Simulation End
Case 1	May 23, 1110	89°–90.5°E, 22.5°–24°N	May 23, 0000	May 24, 0000
Case 2	June 21, 1130	89°–90.5°E, 24°–25.5°N	June 20, 1800	June 21, 1800
Case 3	June 30, 1200	88.5°–90°E, 22.5°–24°N	June 29, 1800	June 30, 1800
Case 4	July 14, 1800	89.5°–91°E, 23.5°–25°N	July 14, 0600	July 15, 0600

2.2 Case Studies and Observational Data

Several intense lightning events that occurred in 2023 are initially considered for analysis, based on observed lightning activity, deep convective development, and associated severe weather phenomena, such as gusty winds, using data from multiple weather stations operated by the Bangladesh Meteorological Department (BMD). From this pool, four representative events are selected for detailed evaluation to capture the diversity of lightning activity across different seasons and convective environments.

Case 1 occurs on 23 May during the pre-monsoon season, when severe local convective storms are climatologically

frequent over Bangladesh (Yamane et al., 2010a). Previous studies show that pre-monsoon convection in this region is favored by strong lower-tropospheric heating (Yamane et al., 2010b; Karmakar and Alam, 2011), abundant low-level moisture that is transported from the Bay of Bengal Yamane et al. (2013), and dynamical lifting associated with low-level convergence. Regional orographic forcing from surrounding elevated terrain may also modulate thunderstorm initiation and propagation over Bangladesh and adjoining northeastern India (Farukh et al., 2023; Sahu et al., 2023, 2024).

Case 2 occurs on 21 June 2023 over northern Bangladesh, during the northward advance and early establishment phase of the southwest monsoon (Akter et al., 2022). Previous studies show that after monsoon onset, southwesterly low-level flow transports abundant moisture from the Bay of Bengal toward inland Bangladesh (Hoque et al., 2011), increasing precipitable water and rainfall potential. This low-level flow pattern is also evident in the 850 hPa wind field from NCEP-NCAR Reanalysis 1 for Case 2 (Figure SI 2). Under such a moist monsoonal environment, mesoscale low-level convergence can provide the lifting needed for deep convection (Farukh et al., 2023), which is consistent with the observed lightning activity in MLX and localized heavy rainfall associated with this case (Figure SI 1).

Cases 3 and 4 occur during the peak monsoon season. Convective systems are more organized, with intense lightning activity distributed over broader regions. Case 4, however, is spatially more confined, featuring localized lightning. This case is selected specifically to assess the model's ability to represent small-scale, high-intensity lightning events. Together, these cases provide a representative sample to evaluate model performance across both widespread and localized lightning occurrences.

To ensure accuracy and temporal precision, these events are further confirmed using near–real-time lightning flash observations from Meteologix (here after MLX), which provides high-resolution detection across Bangladesh with a spatial resolution of 1 km and a temporal frequency of 1–5 minutes.

The convective environment is further characterized using INSAT-3D satellite-based cloud data from the Meteorological and Oceanographic Satellite Data Archival Centre (MOSDAC). It provides multi-sensor observations, including infrared and visible imagery, with temporal resolutions of 15–30 minutes and spatial resolutions of 1–3 km, enabling detailed monitoring of intense convective systems. The MOSDAC thermal-infrared brightness temperature is used to identify deep convective cloud systems associated with the lightning events. In infrared satellite imagery, low brightness temperature represents cold cloud-top temperature, which is generally associated with high cloud tops and vertically developed convective clouds (Lima et al., 2019; Sherwood et al., 2004). Both MOSDAC and MLX datasets are quality-controlled and cross-validated against BMD ground-based measurements to ensure reliability and representativeness for analyzing severe lightning events. The observational datasets are used to evaluate whether the WRF-Elec simulations reproduce the observed convective and lightning signatures for the selected cases. MOSDAC thermal-infrared brightness temperature is used to identify cold cloud-top regions associated with deep convective cloud development, while MLX lightning observations are used to identify the timing and location of observed lightning activity. We use 700 hPa relative humidity and total cloud cover fields from the NCEP–NCAR Reanalysis 1 dataset for the selected lightning cases. These fields are used as an independent reanalysis-based reference to evaluate whether the WRF-Elec simulations reproduce the pre-event mid-tropospheric moisture environment and the cloud-cover conditions during the observed lightning periods. Since WRF does not provide a direct diagnostic of total cloud cover equivalent to that available in the NCEP-NCAR reanalysis, we estimated total cloud cover from the model's low, middle, and high cloud fraction diagnostics using a random overlap assumption. Under this assumption, cloud layers are considered randomly distributed in the vertical, and the total cloud cover is computed as $C_{\text{total}} = 1 - (1 - C_{\text{low}})(1 - C_{\text{mid}})(1 - C_{\text{high}})$, where C_{low}, C_{mid}, and C_{high} are the cloud fractions in the low, middle, and high atmospheric layers, respectively. The resulting cloud cover is expressed as a percentage and compared with the NCEP-NCAR total cloud cover over the same domain and analysis period

The four finalized cases are summarized in Table 2, including the date, time of peak lightning activity (UTC), and the 1.5° × 1.5° latitude–longitude coordinate used for area-averaged analysis. These spatiotemporal windows capture the core regions of convective activity and lightning development for each event, allowing a consistent comparison between model simulations and observations. The forecast lead time is estimated using the area-averaged time series of WRF-Elec outputs within the selected 1.5° × 1.5° analysis coordinate for each case. The observed lightning occurrence time is first identified from the lightning observation data. Subsequently, the temporal evolution of simulated parameters is examined at each model output time. The lead time is defined as the time difference between the observed lightning occurrence and the first clear increase in these microphysical predictors within the analysis coordinate. Thus, the reported lead time represents the period during which the model first indicates favorable storm-growth and lightning-related microphysical conditions prior to the observed lightning event.

3 Results & Discussions

The performance of the integrated lightning forecasting framework is analyzed by combining microphysical parameters: maximum reflectivity, LPI and Lightning Flash Density (LFD) with thermodynamic fields: most unstable CAPE (mCAPE),

most unstable CIN (mCIN), vertical velocity, KI, and TTI. The simulated predictors represent different stages of thunderstorm evolution. Thermodynamic indices describe the pre-convective environment; for example, mCAPE often reaches high values several hours before the event and then decreases as convection develops and instability is consumed, while mCIN generally weakens prior to convective initiation Tuckman et al. (2023). In contrast, microphysical variables are linked to the developing storm structure. Maximum reflectivity, defined as the column-maximum simulated radar reflectivity derived from the model's microphysical scheme, indicates the presence of deep convection, which may subsequently develop into a thunderstorm and produce a lightning event Mohan et al. (2021). A rise in maximum reflectivity before the observed lightning time therefore indicates the formation of the convective core that precedes electrification and discharge. LPI represents the potential for charge separation in the mixed-phase region, whereas LFD represents the model-simulated lightning discharge after sufficient electrification and electric-field development McCaul Jr et al. (2009). Thus, LFD is a later-stage diagnostic than reflectivity and LPI, and its maximum may occur near, before, or after the observed lightning reference time depending on storm timing, propagation, and movement across the domain Barthe et al. (2010).

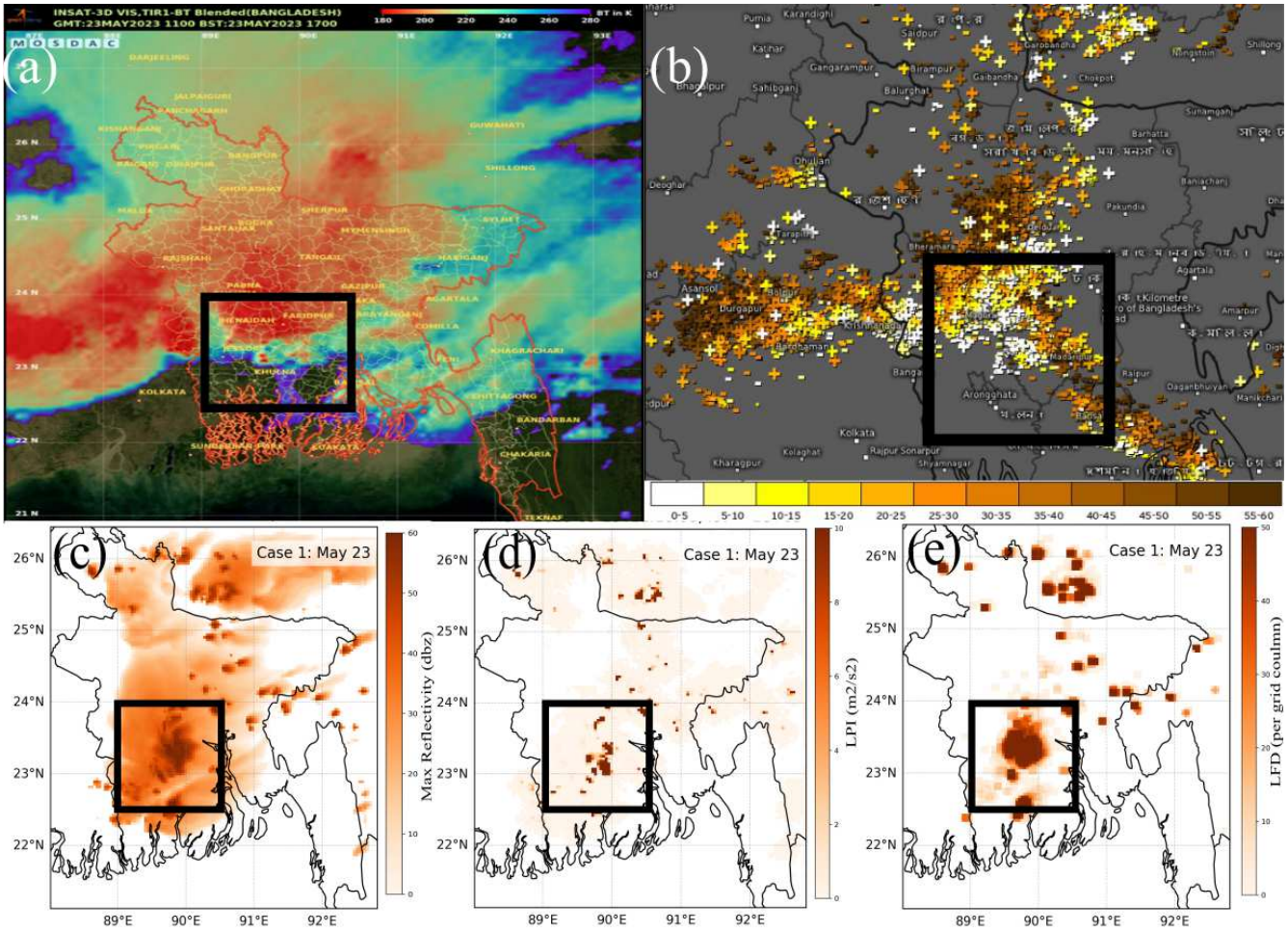


Figure 1: Observation and simulated variables for case 1: May 23. (a) cloud top brightness temperature from MOSDAC at 1100 UTC, (b) lightning flash analysis from MLX at 1115 UTC, (c) maximum reflectivity from WRF simulation at 1110 UTC, (d) same as panel-c but for LPI, (e) same as panel-c but for LFD. The back triangle in each panel are the representative area of the case coordinate mention in Table 2

To begin, we examine the individual properties of the microphysical and thermodynamic fields for each case. In Figure 1a, the area enclosed by the black rectangle exhibits very low brightness temperatures from MOSDAC, indicating the presence of deep convective clouds and substantial hydrometeor loading conditions that are highly favorable for electrification. The lightning analysis product from MLX further confirms active lightning during this period (Figure 1b). Correspondingly, the WRF-Elec simulated fields show a markedly strong response, with maximum reflectivity reaching 60 dBZ, which indicates intense precipitation and strong mixed-phase hydrometeor interactions associated with active convection. LPI values reaching around 10 J kg^{-1} represent the strength of charge separation processes within convective clouds and are commonly used as an indicator of lightning initiation potential. In addition, LFD exceeding 50 flashes per grid column provides a direct estimate of

lightning activity intensity within the black triangle highlighted in Figures 1c-1e. These simulated features accurately capture both the spatial organization and timing of the observed lightning activity with high fidelity.

For Case 2 (Figure SI 1), the MOSDAC brightness temperature field again reveals a pronounced region of cold cloud tops within the analysis domain, suggesting deep convective development. The lightning observations from MLX show active electrical discharges concentrated within the same region, consistent with the satellite-indicated convective cores. The WRF-Elec simulations reproduce these features with enhanced reflectivity values exceeding 45-55 dBZ and elevated LPI values around 10 m^2 s^{-2}, indicating favorable conditions for lightning like case 1. The simulated LFD (Figure SI 4) shows organized clusters that align well with the observed lightning distribution, demonstrating the ability of the model to capture the evolving microphysical structure of the convective system.

Similar agreement is found in the third case, however, the fourth case shows significant discrepancies. Specifically, the model produces very low LPI and LFD values, approximately 1 m^2 s^{-2} and fewer than 10 flashes per grid column, respectively, indicating an underestimate of lightning-related microphysical processes (Figures SI 4 and SI 5). In contrast, case 4 observations (Figure SI 1) show very cold brightness temperatures and active lightning discharges with a strongly confined spatial distribution during this period.

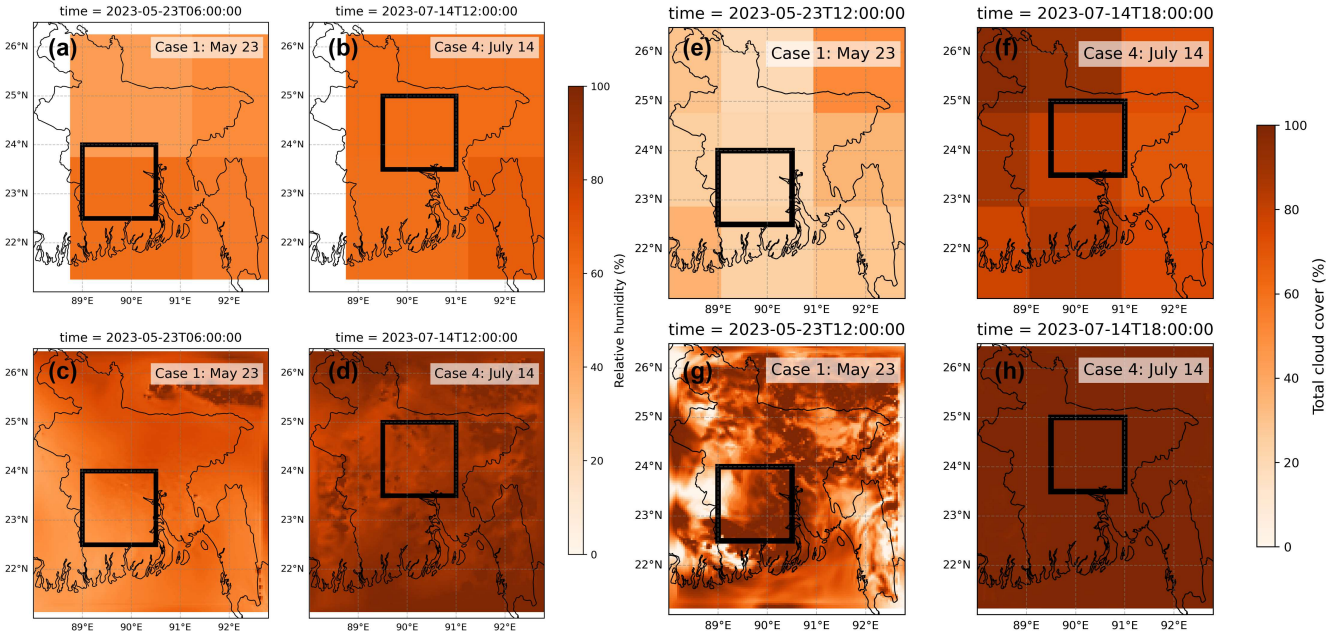


Figure 2: Comparison of NCEP–NCAR Reanalysis 1 and WRF-simulated environmental fields for selected lightning cases. Panels (a–d) show 700 hPa relative humidity (%), while panels (e–h) show total cloud cover (%). The top row in each group represents the NCEP–NCAR Reanalysis 1 fields, and the bottom row represents the corresponding WRF model simulations. Panels (a,c,e,g) correspond to Case 1, and panels (b,d,f,h) correspond to Case 4.

Before examining the microphysical parameters, we first assess whether the model reproduces the broader environmental conditions associated with the selected events. We compare the 700 hPa relative humidity and total cloud cover simulated by the model with the corresponding fields from the NCEP-NCAR Reanalysis 1 dataset for Case 1 and Case 4. As shown in Figure 2, the reanalysis fields indicate a moist mid-tropospheric environment approximately 6 hours prior to the event and enhanced cloud cover within and around the selected coordinate during the event periods. The WRF simulations reproduce these broad moisture and cloud-cover patterns reasonably well, suggesting that the model is capable of capturing favorable environmental signals for convective development. Although differences in magnitude and spatial detail are expected due to the coarse resolution of the reanalysis data and the higher-resolution WRF simulation, the overall consistency supports the use of the model output for the study.

To better understand the contrasting lightning responses in Cases 1 and 4, we examine the graupel water path (GWP), ice water path (IWP), and vertical velocity within the mixed-phase region. These variables provide complementary information on the microphysical and dynamical conditions required for electrification. Figure 3 shows that, in Case 1, both GWP and IWP exhibit pronounced maxima within the coordinate, indicating abundant mixed-phase hydrometeors within the convective core. The strong graupel and ice signals suggest favorable conditions for non-inductive charge separation, which is a key process for storm electrification and lightning development. This is further supported by the vertical velocity structure in Figure 4, where a stronger upward motion is found within and near the coordinate. The corresponding latitude-pressure cross-section

shows a deeper and more coherent updraft extending through the mid-troposphere and intersecting the 0°C level, indicating efficient vertical transport of hydrometeors into the mixed-phase layer. These conditions are consistent with the enhanced LPI and LFD responses simulated for Case 1.

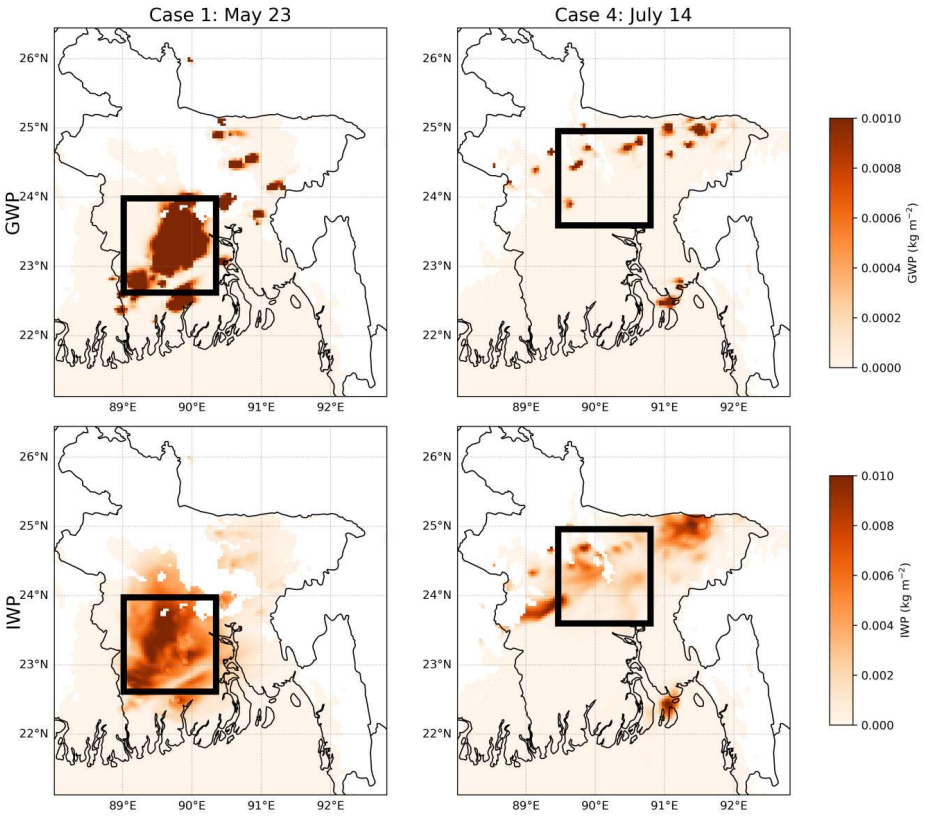


Figure 3: Model-simulated graupel water path (GWP; top row) and ice water path (IWP; bottom row) for Case 1 and Case 4.

In contrast, Case 4 shows a much weaker and more dispersed GWP distribution within the coordinate, whereas the IWP field is more diffuse and partly displaced from the analysis box. The vertical velocity field also shows weaker and more scattered upward motion, with limited vertical continuity through the mixed-phase layer compared to case 1. This suggests that the model does not adequately simulate the localized convective intensity required for strong mixed-phase hydrometeor growth, graupel–ice interaction, and charge separation. Therefore, the reduced GWP, weak updraft structure, and limited mixed-phase development help explain the weak LPI and LFD signals in Case 4. This discrepancy suggests that the model struggles to adequately resolve the dynamical and microphysical processes in highly localized systems, where strong convection and electrification occur over limited spatial scales. In general, this emphasizes the role of microphysical parameters and demonstrates the ability of the model to represent the essential physical processes governing the initiation of lightning, while acknowledging its limitations in capturing highly localized convective structures.

Since microphysical fields provide more localized lightning signals, we next analyze area weighted localize mean profile within the 1.5×1.5 deg spatial coordinate for each case to evaluate the potential lead time for forecasting lightning. In the top row of Figure 5, max reflectivity, LPI, and LFD begin to increase around 08:50 UTC that is two and half hours prior to the actual lightning event for case 1. For the remaining cases, these microphysical indicators start rising between three and six hours before the lightning occurrence. In contrast, the fourth case exhibits very low LPI and LFD values throughout the temporal evolution compared to first three cases, which is consistent with the spatial analysis where these indicators are completely missed by the model. This shows that the temporal evolution of maximum reflectivity, LPI, and LFD can provide an early warning signal with a lead time of approximately two to six hours for convective electrification within a 1.5×1.5 deg spatial coordinate, particularly for cases characterized by larger spatial development of thundercloud systems. This again highlight the limitation of the model in simulating confined, small-scale convective events, where temporal signals of lightning activity may be substantially underestimated. Overall, the analysis illuminates the potential utility of microphysical parameters for short-term to medium-term lightning forecasting and offers insights into the timing of convective processes relative to observed lightning events.

We next examine the performance of thermodynamic parameters for lightning forecasting. We find that these thermody-

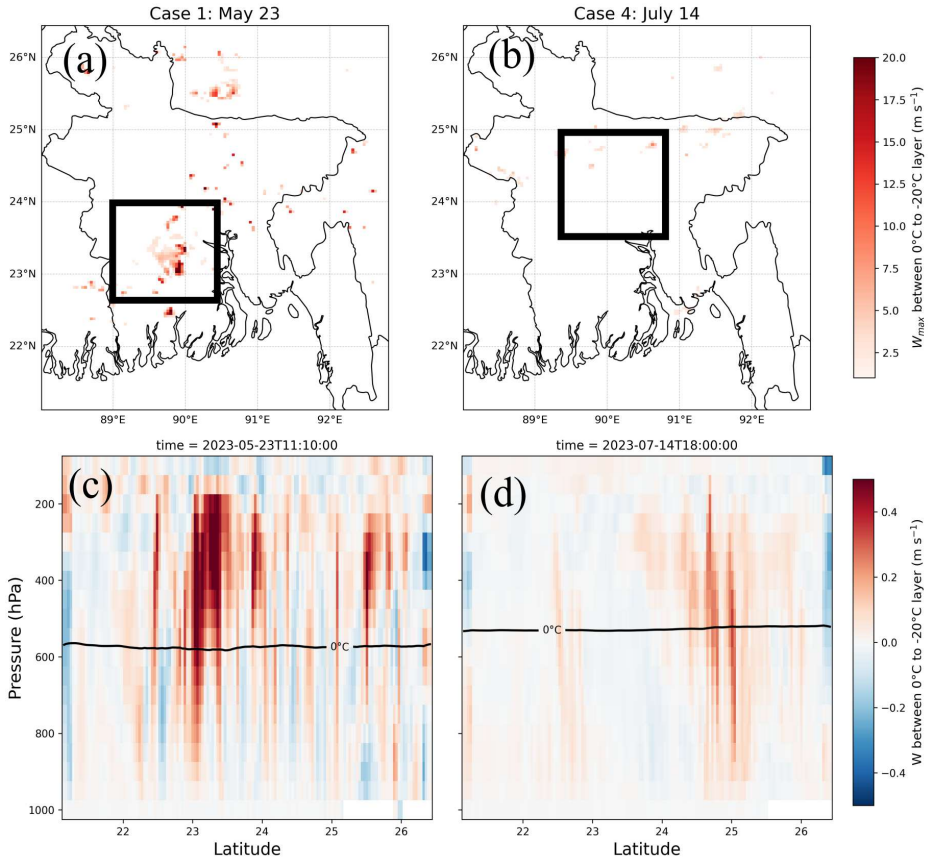


Figure 4: Spatial distribution of maximum vertical velocity W_{max} within the 0–20°C mixed-phase layer (a, b) and associated meridional cross sections (c, d). The black rectangles in top panels indicate the case coordinate and the black contour marks the 0°C isotherm in lower panels.

namic indices exhibit signals much earlier (Figure 6) but with less precise spatial information (Figure SI 6). For instance, in Case 1, mCAPE increases substantially and reaches values of approximately 3000 J kg^{-1} about 10 hours before the beginning of the observed lightning event. This high value of mCAPE indicates the presence of sufficient buoyant energy to support strong updraft development, which is a key ingredient for deep convective and thunderstorm activity. During the same period, mCIN remains relatively low, with values below 50 J kg^{-1}. Low mCIN values suggest that only minimal energy is required to initiate parcel ascent, thereby allowing convection to develop more readily. The simultaneous occurrence of high mCAPE and low mCIN therefore represents thermodynamic conditions that are highly favorable for thunderstorm initiation and subsequent electrification processes.

Similarly, for Case 1, vertical velocity reaches peak values approximately 3 hours before the lightning event, indicating the strengthening of convective updrafts. The KI starts rising about 6 hours prior to the event, while the TTI values are elevated roughly 3 hours before lightning occurrence, both suggesting enhanced atmospheric instability and moisture availability favorable for deep convection.

For Cases 2 through 4, vertical velocity consistently peaks within two to four hours before lightning occurrence, highlighting the transition from favorable environmental conditions to active convective development. In comparison, both the K-Index (KI) and Total Totals Index (TTI) reach elevated values nearly 10-12 hours before the lightning events, indicating that large-scale thermodynamic conditions supportive of convection are established well in advance. A transient behavior appears in case 2, mCAPE drops to a near-zero value during a single model output interval and likely reflects the rapid transition of the thermodynamic environment during convective initiation. However, because the signal is confined to one output time, some contribution from the temporal resolution of the diagnostic calculations cannot be ruled out. Overall, these results suggest that thermodynamic indices provide longer lead-time signals, whereas vertical velocity captures the immediate dynamical intensification preceding lightning activity.

However, all of the thermodynamic fields exhibit broadly elevated values across the entire spatial domain, indicating favorable conditions for convection but offering little guidance on the precise location of lightning activity (Figure SI 6). In case 1, the mCAPE map at 10 UTC shows uniformly high values across nearly the entire Bangladesh region, with magnitudes

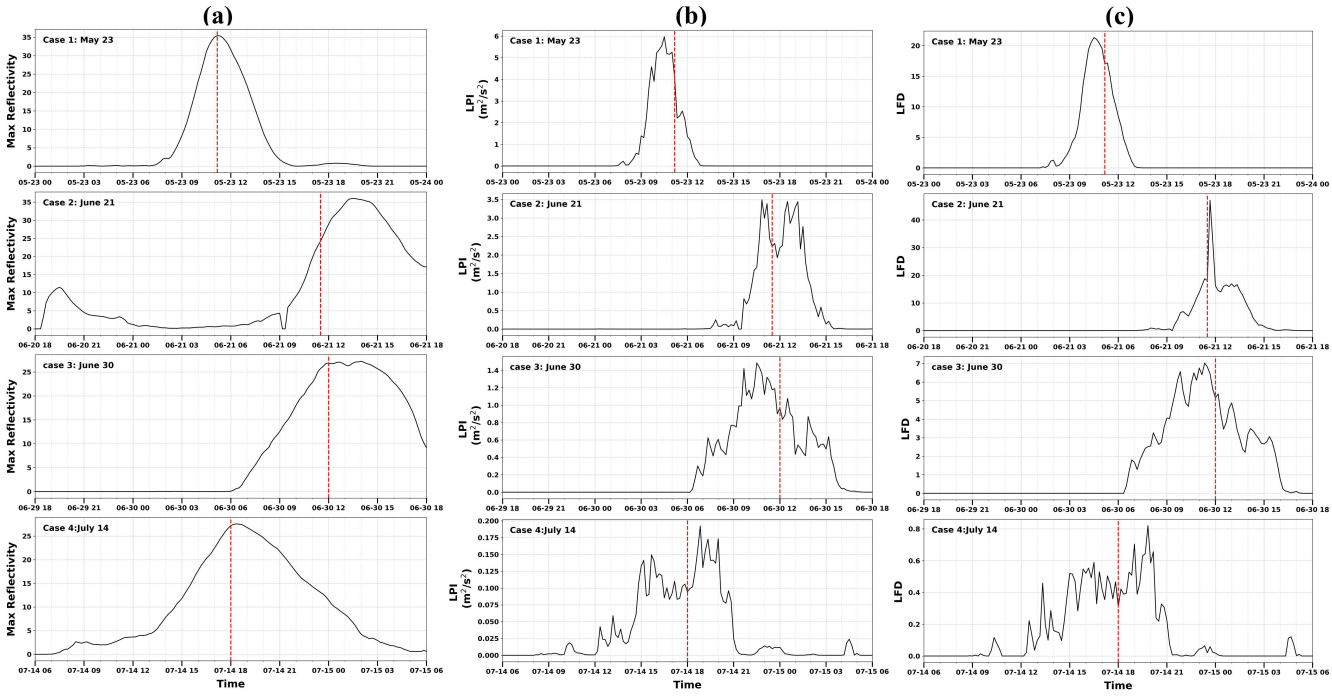


Figure 5: Model simulated weighted area-average (a) maximum reflectivity (b) LPI and (c) LFD for the four case studies, with each row corresponding to one case. The dashed red vertical line represents the time of actual event. X-axis ticks are labeled as MM-DD HH UTC. The averaging domains are defined in Table 2

approaching 4000 J kg^{-1}. Similarly, both the KI and TTI display widespread values ranging than 40-50 ^0C over the full domain. While these high values clearly indicate an environment conducive to deep convection and thunderstorm development, they do not provide sufficient spatial separation to identify likely region of lightning activity. This highlights the limitation of relying solely on large-scale thermodynamic indicators for lightning prediction.

These results highlight that thermodynamic indices are valuable for early warnings but lack spatial specificity. This same conclusion has also been found for thermodynamic fields in recent studies (Paul et al., 2019; Johns and Doswell III, 1992; Rajasekhar et al., 2016). Therefore, coupling microphysical and thermodynamic indicators can deliver both longer lead times and precise spatial predictions. To further examine the effectiveness of the integrated framework, we construct a combined diagnostic field using LPI and mCAPE. Figure 7 shows that the combined LPI-mCAPE field captures the main lightning-prone regions for all four cases. For Cases 1–3, the combined diagnostic remains consistent with the strong LPI and LFD signals discussed earlier, indicating that active microphysical development coincides with favorable instability. More importantly, in Case 4, where LPI and LFD alone are weak and fail to clearly represent the localized lightning activity, the combined LPI–mCAPE field shows a more distinct signal. This suggests that although the model underestimates the explicit microphysical lightning response in this localized event, combining thermodynamic instability with microphysical parameters still provides meaningful information on the potential for convective development and lightning occurrence.

In this study, we implement, for the first time, an integrated approach that simultaneously utilizes microphysical (Figure 5) and thermodynamic (Figure 6) information. Although thermodynamic instability indices and WRF-based microphysical diagnostics have been used in previous thunderstorm and lightning studies, their complementary roles in lightning prediction have not been systematically examined. Previous studies have demonstrated the potential of WRF-based lightning prediction, but they have primarily focused on the ability of WRF-Elec to simulate lightning events and evaluated the predictive skill of lightning predictors (Paul et al., 2022; Rabbani et al., 2022; Paramanik et al., 2024) rather than on how thermodynamic and microphysical indicators can be combined to improve both forecast lead time and spatial localization. The combined LPI–mCAPE diagnostic in (Figure 7) further supports this integrated framework by showing that although LPI alone fails to clearly represent the lightning event for case 4, combined diagnostic produces a more distinct and spatially consistent signal, demonstrating the added value of integrating microphysical and thermodynamic predictors. The integrated assessment of these two groups of predictors demonstrate that thermodynamic fields provide early indications of favorable environmental conditions, whereas WRF-Elec microphysical fields offer more spatially localized information on lightning occurrence. This framework enables lightning prediction with a lead time of 3–6 hours and a spatial coverage of approximately 1.5° × 1.5°, thereby improving both the temporal and spatial accuracy of short-term lightning forecasts.

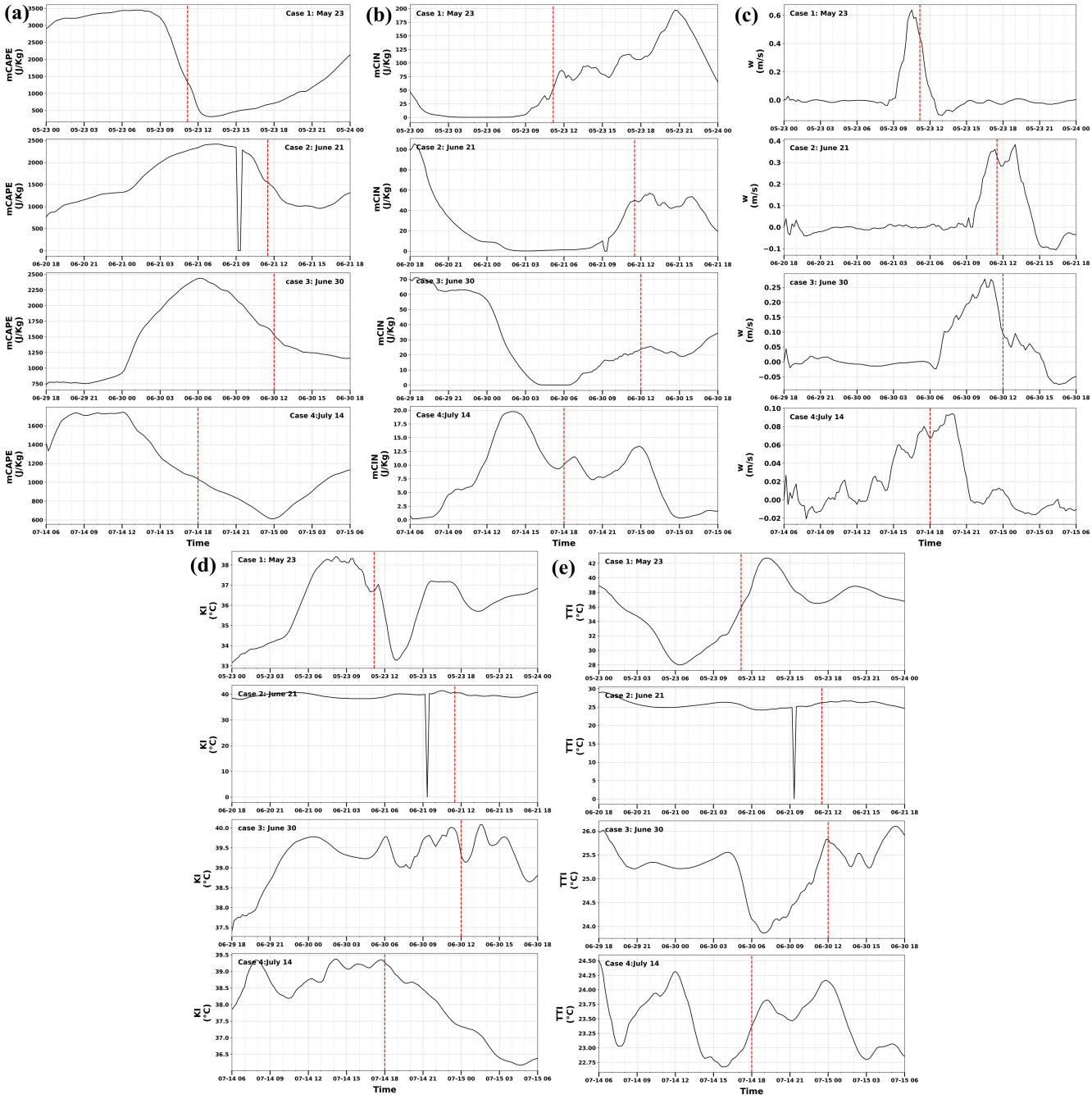


Figure 6: Same as Figure 5 but for (a) mCAPE, (b) mCIN, (c) vertical velocity (w) at 500hPa, (d) KI and (e) TTI

For example, in Case 3, maximum reflectivity, LPI, and LFD begin to increase approximately six hours before the actual lightning activity within the coordinate boundary, indicating the growing stage of hydrometeor (e.g., hail, graupel). In addition, we find favorable values for convection such as significantly high mCAPE, low mCIN, high vertical velocity, rising KI, and rising TTI roughly ten hours prior to the event. The combination of microphysical and thermodynamic information allows us to achieve both longer lead times and higher spatial accuracy in lightning prediction. By jointly considering these two types of information, the model can better capture the initiation and evolution of convective events, improving the timing and location of predicted lightning activity.

In another example, Case 1 illustrates the complementary strengths of the two datasets: microphysical fields provide a lead time of 2–3 hours, while thermodynamic fields indicate consistently favorable conditions for thunderstorm development up to 6–10 hours before the event. Together, these fields allow for early detection and accurate spatial characterization of lightning activity, which is not achievable when using microphysical or thermodynamic information alone. Overall, the

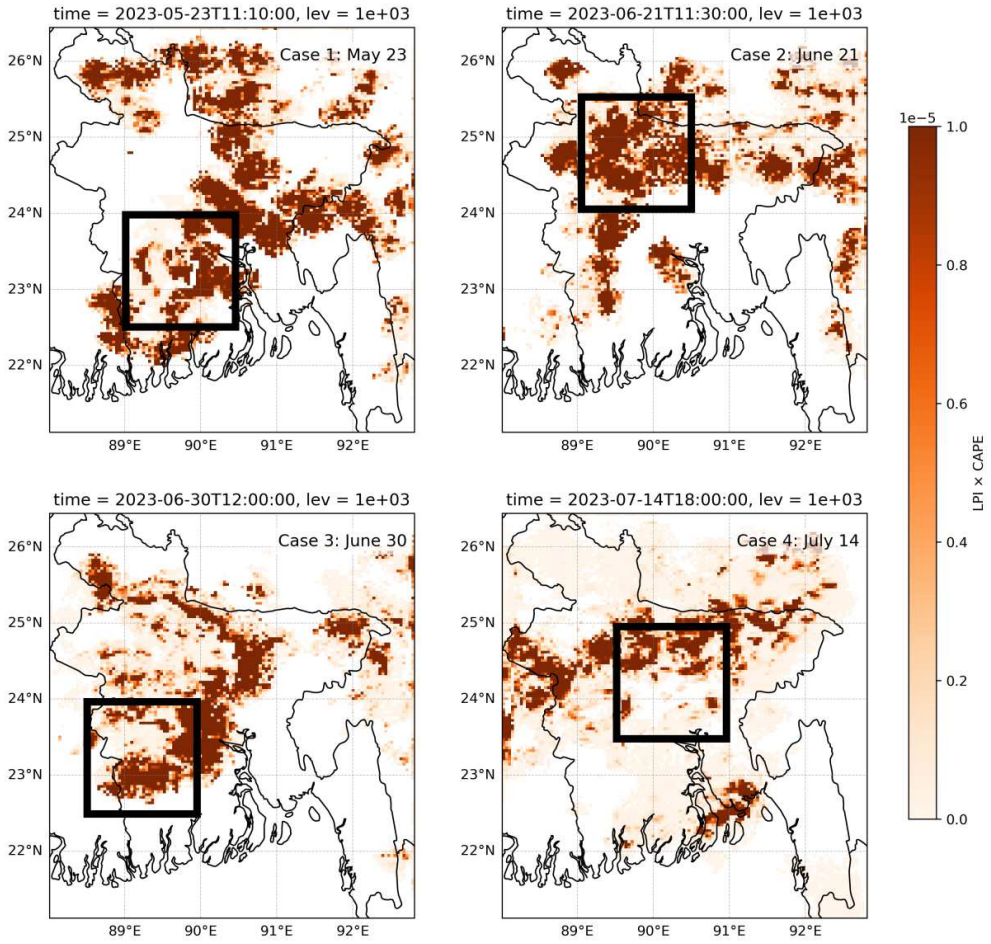


Figure 7: Combined LPI–mCAPE map for four cases at the time of the case

integrated approach consistently enhances both the temporal and spatial predictability of lightning events across multiple cases, highlighting its potential as a robust tool for short-term lightning forecasting.

4 Conclusions

In this study, for the first time, we present an integrated framework that combines microphysical and thermodynamic indicators to improve short-term lightning prediction. Our analysis demonstrates that microphysical parameters, specifically LPI, LFD, and radar reflectivity alone are capable of predicting lightning activity with remarkable spatial and temporal accuracy, providing a reliable lead time of approximately 2–6 hours. In contrast, thermodynamic parameters such as mCAPE, mCIN, vertical velocity (w), KI, and TTI exhibit predictive skill over a longer horizon of up to 10–12 hours, but their forecasts lack precise locational information. This limits their utility for targeted warning systems. By strategically combining both microphysical and thermodynamic predictors, we achieve a synergistic effect: the integrated approach not only extends the effective lead time to 3–6 hours but also preserves the spatial specificity necessary for actionable forecasts. This combined methodology therefore offers a significant improvement over relying on either predictor type alone, enabling both higher-confidence lightning predictions and precise localization. The results underscore the importance of leveraging complementary atmospheric information to optimize forecasting capability, suggesting that hybrid predictive frameworks can provide both advanced warning and spatially resolved guidance, which is crucial for risk mitigation and operational decision-making in severe weather scenarios.

The current study focuses on four severe lightning events over Bangladesh, this framework can be extended to regions with complex terrain or different climatological conditions, and the approach is inherently transferable to other datasets and operational forecasting systems. Limitations arise when lightning events are confined to very small areas, where the WRF model may fail to fully capture microphysical indicators such as LPI and LFD, potentially reducing predictive skill. These limitations could be addressed by using higher-resolution simulations, smaller grid boundaries, or alternative initial and boundary

datasets such as GFS for real-time implementation. Furthermore, a more robust assessment will require a larger set of events and standardized verification metrics such as probability of detection (POD), false alarm ratio (FAR), and critical success index (CSI).

Overall, this study represents an important step toward a generalizable, integrated lightning prediction framework. Beyond the local context of Bangladesh, the approach demonstrates how coupling microphysical and thermodynamic information can enhance both temporal and spatial predictability of convective activity. The framework has the potential to be applied to other regions and operational settings, offering a pathway for advancing short-term lightning forecasts and contributing to broader understanding and management of severe convective events.

Declarations

Funding

No specific funding was received for this research.

Conflicts of Interest

The authors declare that they have no known competing financial interests or personal relationships that could have influenced the work reported in this paper.

Availability of Data and Materials

The datasets generated and/or analyzed during the current study are available from the corresponding author on reasonable request.

Authors' Contributions

PP contributed to the study conception, methodology development, model simulations, data analysis, interpretation of results, and manuscript writing. JFJ contributed to the analysis and interpretation of the initial results. Both authors reviewed and approved the final manuscript.

References

Ahasan, M., Rashid, T., Quadir, D., Sultana, S., 2021. Simulation of a hailstorm event over bangladesh using wrf model. The Dhaka University Journal of Earth and Environmental Sciences , 123–130.

Akter, S., Rashid, T., Quadir, D.A., Ahasan, M.N., Shuvo, S.D., Hasan, M.S., 2022. Study of arrival and withdrawal of southwest summer monsoon over bangladesh and analysis of extreme early and late arrival events using regcm. The Dhaka University Journal of Earth and Environmental Sciences 11, 101–111.

Barthe, C., Deierling, W., Barth, M.C., 2010. Estimation of total lightning from various storm parameters: A cloud-resolving model study. Journal of Geophysical Research: Atmospheres 115.

Bondyopadhyay, S., Mohapatra, M., 2023. Determination of suitable thermodynamic indices and prediction of thunderstorm events for eastern india. Meteorology and Atmospheric Physics 135, 4.

Christian, H.J., Blakeslee, R.J., Boccippio, D.J., Boeck, W.L., Buechler, D.E., Driscoll, K.T., Goodman, S.J., Hall, J.M., Koshak, W.J., Mach, D.M., et al., 2003. Global frequency and distribution of lightning as observed from space by the optical transient detector. Journal of Geophysical Research: Atmospheres 108, ACL–4.

Dewan, A., Hossain, M.F., Rahman, M.M., Yamane, Y., Holle, R.L., 2017. Recent lightning-related fatalities and injuries in bangladesh. Weather, climate, and society 9, 575–589.

Farukh, M.A., Islam, M.A., Uddin, M.N., 2023. Synoptic climatology of pre-monsoon frequent lightning events in bangladesh. Natural Hazards 116, 1053–1070.

Ferdaus, J., Quadir, D.A., Alam, M.S., Panda, S.K., Das, S., Ahasan, M.N., Rabbani, K.M.G., Shuvo, S.D., 2021. Prediction of thunderstorms based on atmospheric instability indices over bangladesh using wrf-arw model. Jalawaayu 1, 21–37.

Fierro, A.O., Mansell, E.R., MacGorman, D.R., Ziegler, C.L., 2013. The implementation of an explicit charging and discharge lightning scheme within the wrf-arw model: Benchmark simulations of a continental squall line, a tropical cyclone, and a winter storm. Monthly Weather Review 141, 2390–2415.

Gharaylou, M., Farahani, M.M., Hosseini, M., Mahmoudian, A., 2019. Numerical study of performance of two lightning prediction methods based on: Lightning potential index (lpi) and electric potential difference (pot) over tehran area. Journal of Atmospheric and Solar-Terrestrial Physics 193, 105067.

Gharaylou, M., Farahani, M.M., Mahmoudian, A., Hosseini, M., 2020. Prediction of lightning activity using wrf-elec model: Impact of initial and boundary conditions. Journal of Atmospheric and Solar-Terrestrial Physics 210, 105438.

Gofa, F., Boucouvala, D., Samos, I., Louka, P., 2023. Lightning potential forecast evaluation and its correlation with thermodynamic indices. Environmental Sciences Proceedings 26, 109.

Hong, S.Y., Noh, Y., Dudhia, J., 2006. A new vertical diffusion package with an explicit treatment of entrainment processes. Monthly weather review 134, 2318–2341.

Hoque, R., Matsumoto, J., Hirano, J., 2011. Climatological characteristics of monsoon seasonal transitions over bangladesh. Geographical Reports of Tokyo Metropolitan University , 31–41.

Iacono, M.J., Delamere, J.S., Mlawer, E.J., Shephard, M.W., Clough, S.A., Collins, W.D., 2008. Radiative forcing by long-lived greenhouse gases: Calculations with the aer radiative transfer models. Journal of Geophysical Research: Atmospheres 113.

Johns, R.H., Doswell III, C.A., 1992. Severe local storms forecasting. Weather and Forecasting 7, 588–612.

Johnson, A., Wang, X., Kong, F., Xue, M., 2013. Object-based evaluation of the impact of horizontal grid spacing on convection-allowing forecasts. Monthly weather review 141, 3413–3425.

Kain, J.S., Weiss, S.J., Bright, D.R., Baldwin, M.E., Levit, J.J., Carbin, G.W., Schwartz, C.S., Weisman, M.L., Droegemeier, K.K., Weber, D.B., et al., 2008. Some practical considerations regarding horizontal resolution in the first generation of operational convection-allowing nwp. Weather and Forecasting 23, 931–952.

Karmakar, S., Alam, M.M., 2011. Modified instability index of the troposphere associated with thunderstorms/nor'westers over bangladesh during the pre-monsoon season. Mausam 62, 205–214.

Kunz, M., 2007. The skill of convective parameters and indices to predict isolated and severe thunderstorms. Natural Hazards and Earth System Sciences 7, 327–342.

Lima, C.B., Prijith, S.S., Sesha Sai, M.V., Rao, P.V., Niranjan, K., Ramana, M.V., 2019. Retrieval and validation of cloud top temperature from the geostationary satellite insat-3d. Remote Sensing 11, 2811.

Lynn, B., Yair, Y., 2008. Lightning potential index: A new tool for predicting the lightning density and the potential for extreme rainfall. Geophysical Research Abstracts, EGU General Assembly, Vienna 10.

Lynn, B., Yair, Y., 2010. Prediction of lightning flash density with the wrf model. Advances in Geosciences 23, 11–16.

Mahapatra, D., Panda, S., Banik, T., Banerjee, B.K., 2026. Performance assessment of wrf-elec and lightning potential index for improved forecasting in odisha, india. Natural Hazards 122, 403.

Mansell, E.R., MacGorman, D.R., Ziegler, C.L., Straka, J.M., 2005. Charge structure and lightning sensitivity in a simulated multicell thunderstorm. Journal of Geophysical Research: Atmospheres 110.

Mansell, E.R., Ziegler, C.L., Bruning, E.C., 2010. Simulated electrification of a small thunderstorm with two-moment bulk microphysics. Journal of the Atmospheric Sciences 67, 171–194.

McCaul Jr, E.W., Goodman, S.J., LaCasse, K.M., Cecil, D.J., 2009. Forecasting lightning threat using cloud-resolving model simulations. Weather and Forecasting 24, 709–729.

Meteologix, . Bangladesh lightning data. https://meteologix.com/bd/lightning. Accessed: 2025-12-03.

Mohan, G.M., Vani, K.G., Hazra, A., Mallick, C., Chaudhari, H.S., Pokhrel, S., Pawar, S., Konwar, M., Saha, S.K., Das, S.K., et al., 2021. Evaluating different lightning parameterization schemes to simulate lightning flash counts over maharashtra, india. Atmospheric Research 255, 105532.

MOSDAC, . Meteorological and oceanographic satellite data archive. https://www.mosdac.gov.in. Accessed: 2025-12-03.

Paramanik, M.M.R., Rabbani, K.M.G., Imran, A., Islam, M.J., Syed, I.M., 2024. Prediction of lightning activity over bangladesh using diagnostic and explicit lightning parameterizations of wrf model. Natural Hazards 120, 4399–4422.

Paul, P., Imran, A., Islam, M.J., Kabir, A., Jaman, S., Syed, I.M., 2019. Study of pre-monsoon thunderstorms and associated thermodynamic features over bangladesh using wrf-arw model. Dhaka University Journal of Science 67, 151–156.

Paul, P., Imran, A., Mallik, M.A.K., Syed, I.M., 2022. Diagnostic study of the lightning potential index and electric field in two thunderstorm cases over bangladesh. Atmospheric and Oceanic Optics 35, 524–540.

Prein, A.F., Langhans, W., Fosser, G., Ferrone, A., Ban, N., Goergen, K., Keller, M., Tölle, M., Gutjahr, O., Feser, F., et al., 2015. A review on regional convection-permitting climate modeling: Demonstrations, prospects, and challenges. Reviews of geophysics 53, 323–361.

Rabbani, K.M.G., Islam, M.J., Fierro, A.O., Mansell, E.R., Paul, P., 2022. Lightning forecasting in bangladesh based on the lightning potential index and the electric potential. Atmospheric Research 267, 105973.

Rajasekhar, M., Sreeshna, T., Rajeevan, M., SSVS, R., et al., 2016. Prediction of severe thunderstorms over sriharikota island by using the wrf-arw operational model, in: Remote sensing and modeling of the atmosphere, oceans, and interactions VI, SPIE. pp. 147–164.

Sahu, R., Tyagi, B., Singh, K.S., Nayak, H.P., 2024. Evaluating the influence of the shillong plateau topography on thunderstorm activity over northeast india .

Sahu, R.K., Nayak, S., Singh, K.S., Nayak, H.P., Tyagi, B., 2023. Evaluating the impact of topography on the initiation of nor'westers over eastern india. Geomatics, Natural Hazards and Risk 14, 2184669.

Schwartz, C.S., Kain, J.S., Weiss, S.J., Xue, M., Bright, D.R., Kong, F., Thomas, K.W., Levit, J.J., Coniglio, M.C., 2009. Next-day convection-allowing wrf model guidance: A second look at 2-km versus 4-km grid spacing. Monthly Weather Review 137, 3351–3372.

Sherwood, S.C., Chae, J.H., Minnis, P., McGill, M., 2004. Underestimation of deep convective cloud tops by thermal imagery. Geophysical Research Letters 31.

Srivastava, A., Kundu, S.S., Pawar, S.D., Gogoi, R.B., Chakravorty, A., Chhari, A., Gopalkrishnan, V., Aggarwal, S.P., 2023. Evaluation of wrf-elec model to forecast lightning over the north eastern region of india. Meteorology and Atmospheric Physics 135, 39.

Tewari, M., 2004. Implementation and verification of the unified noah land surface model in the wrf model. (No Title) .

Tuckman, P., Agard, V., Emanuel, K., 2023. Evolution of convective energy and inhibition before instances of large cape. Monthly Weather Review 151, 321–338.

Vani K, G., Mohan, G.M., Hazra, A., Pawar, S., Pokhrel, S., Chaudhari, H.S., Konwar, M., Saha, S.K., Mallick, C., Das, S.K., et al., 2022. Evaluation and usefulness of lightning forecasts made with lightning parameterization schemes coupled with the wrf model. Weather and Forecasting 37, 709–726.

Yair, Y., Lynn, B., Price, C., Kotroni, V., Lagouvardos, K., Morin, E., Mugnai, A., Llasat, M.d.C., 2010. Predicting the potential for lightning activity in mediterranean storms based on the weather research and forecasting (wrf) model dynamic and microphysical fields. Journal of Geophysical Research: Atmospheres 115.

Yamane, Y., Hayashi, T., Dewan, A.M., Akter, F., 2010a. Severe local convective storms in bangladesh: Part i. climatology. Atmospheric Research 95, 400–406.

Yamane, Y., Hayashi, T., Dewan, A.M., Akter, F., 2010b. Severe local convective storms in bangladesh: Part ii.: Environmental conditions. Atmospheric Research 95, 407–418.

Yamane, Y., Hayashi, T., Kiguchi, M., Akter, F., Dewan, A.M., 2013. Synoptic situations of severe local convective storms during the pre-monsoon season in bangladesh. Int. J. Climatol 33, 725–734.

Zhuo, L., Dai, Q., Han, D., Chen, N., Zhao, B., 2019. Assessment of simulated soil moisture from wrf noah, noah-mp, and clm land surface schemes for landslide hazard application. Hydrology and Earth System Sciences 23, 4199–4218.

Ziegler, C.L., MacGorman, D.R., 1994. Observed lightning morphology relative to modeled space charge and electric field distributions in a tornadic storm. Journal of Atmospheric Sciences 51, 833–851.

Ziegler, C.L., MacGorman, D.R., Dye, J.E., Ray, P.S., 1991. A model evaluation of noninductive graupel-ice charging in the early electrification of a mountain thunderstorm. Journal of Geophysical Research: Atmospheres 96, 12833–12855.

Supplementary Information (SI)

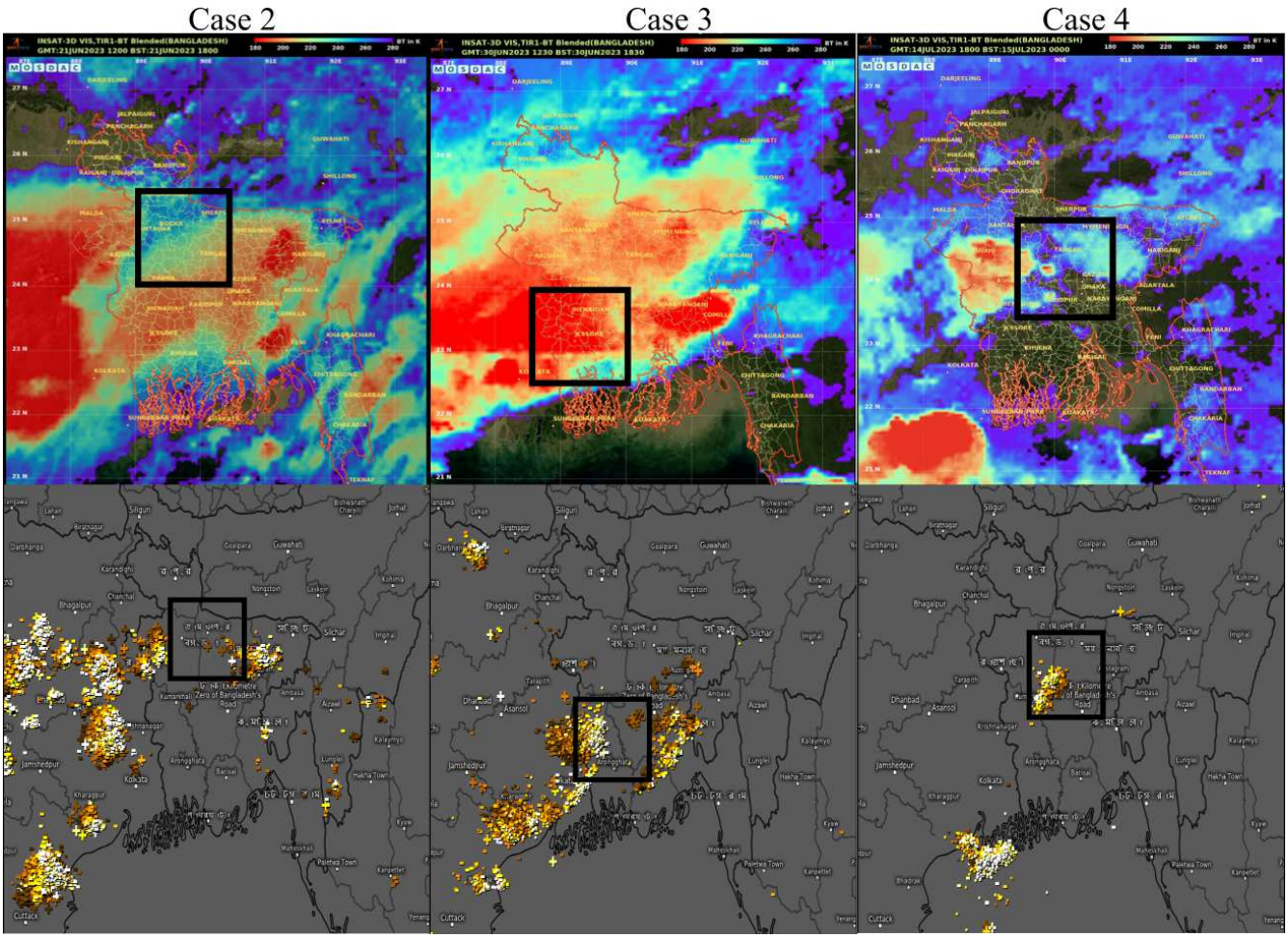


Figure SI 1: MOSDAC and Metologix observations for case 2-4

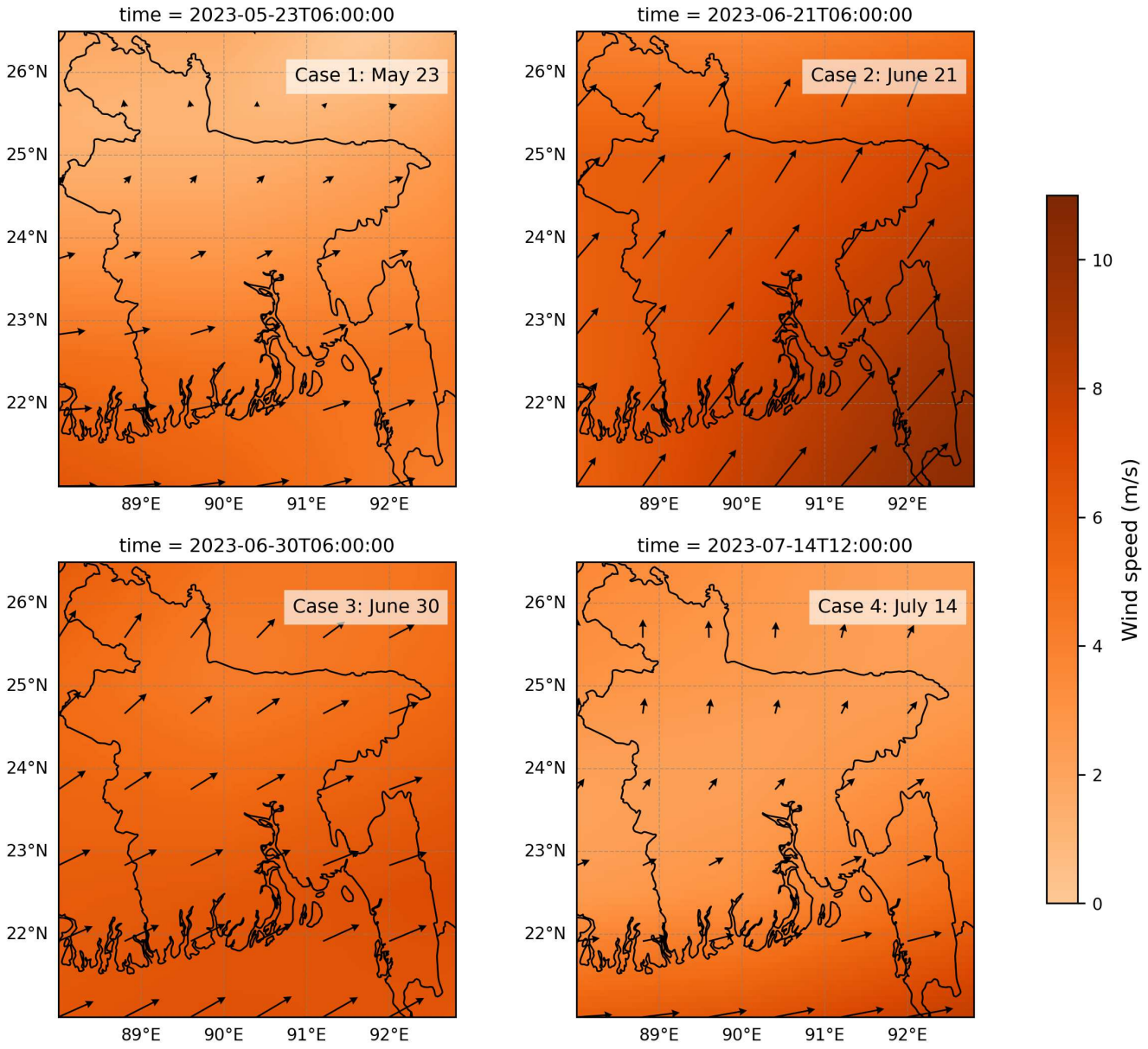


Figure SI 2: NCEP-NCAR Reanalysis 1 850 hPa wind vectors and wind speed for the four selected lightning cases. The vectors show the low-level wind direction, while the shading represents wind speed

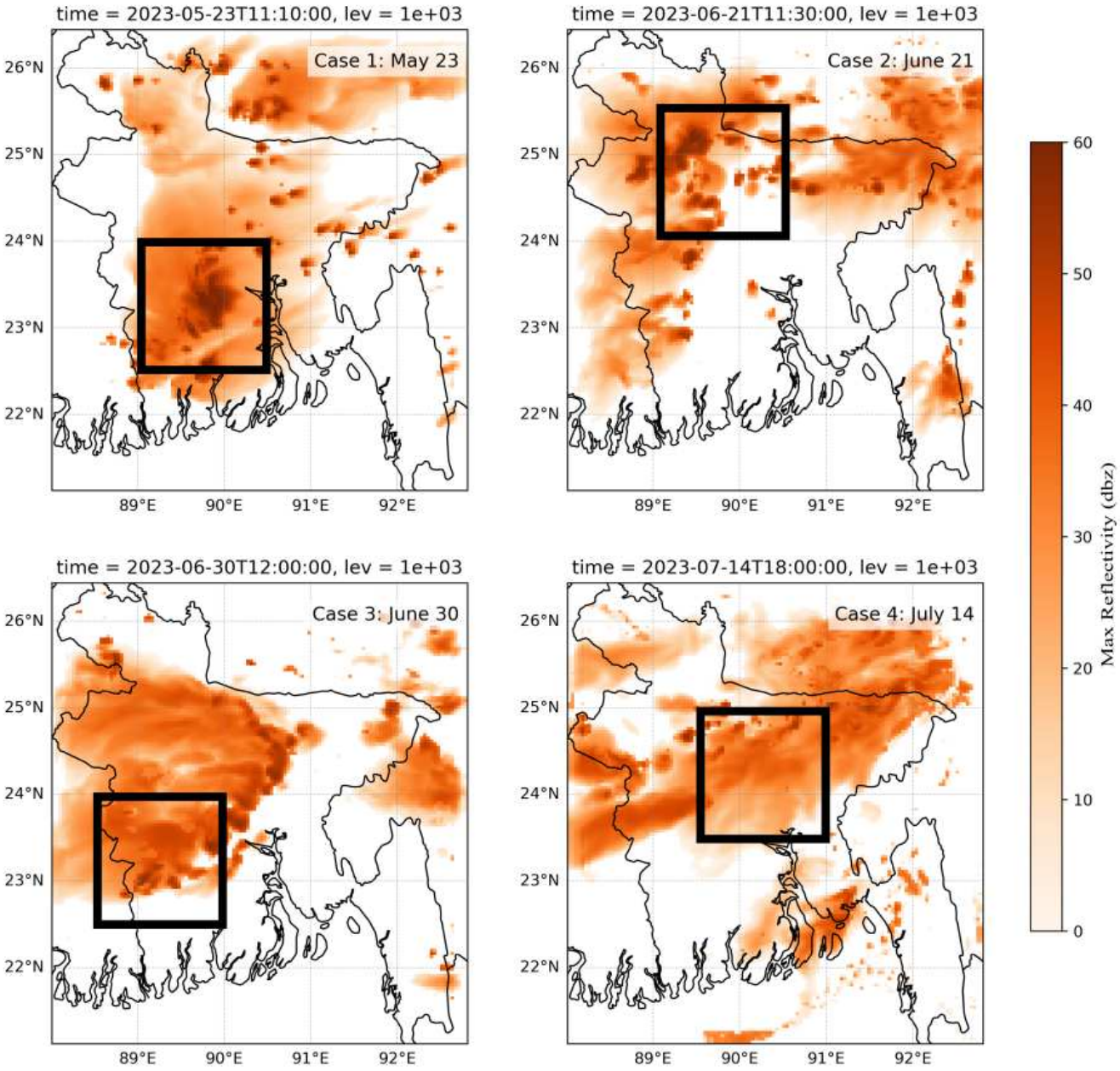


Figure SI 3: Max Reflectivity map for four cases at the time of case. The back triangle is the representative area of the case coordinate mention in Table 2

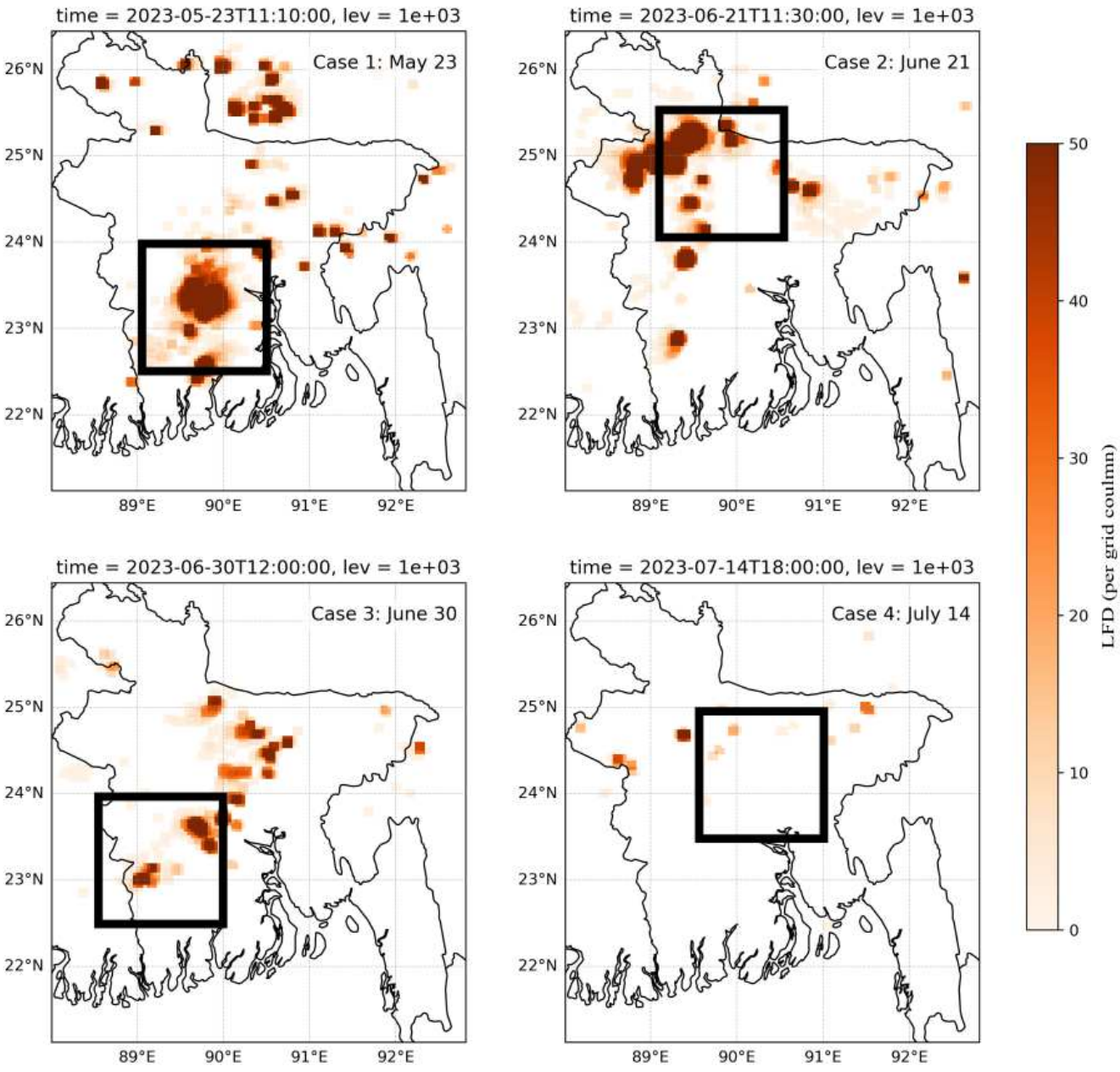


Figure SI 4: Same as Figure SI 1 but for LFD

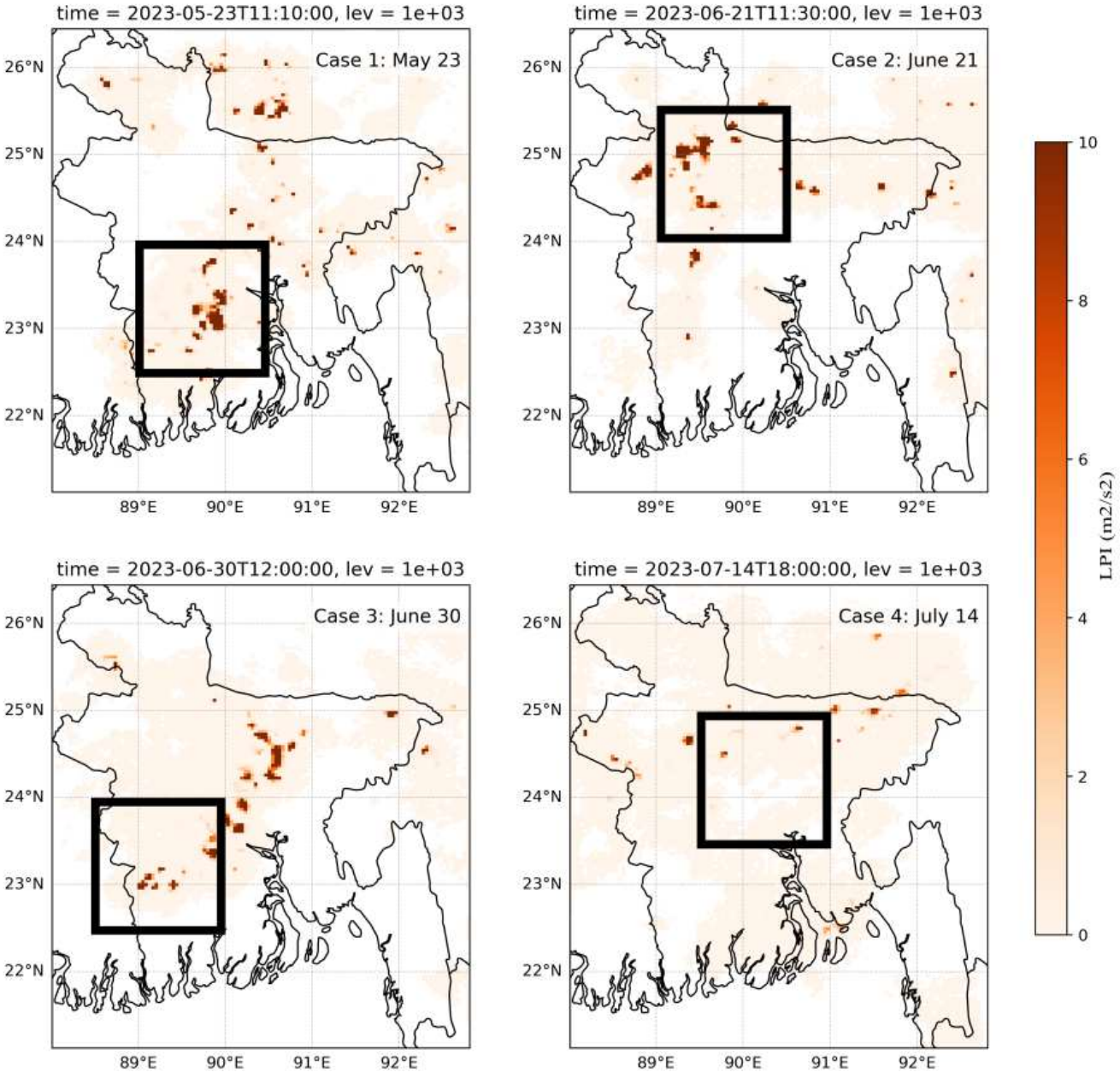


Figure SI 5: Same as Figure SI 1 but for LPI

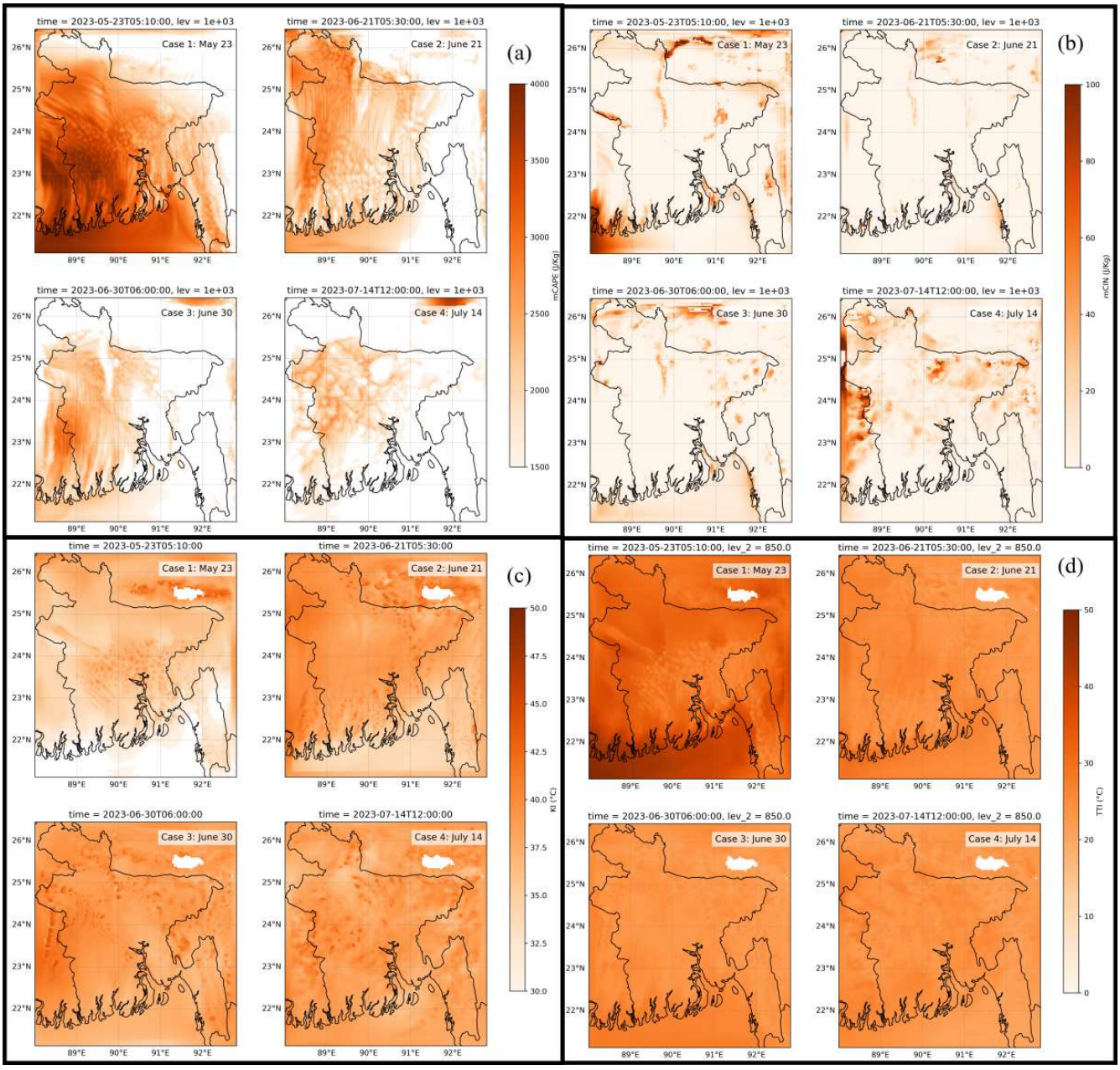


Figure SI 6: Model Simulated thermodynamic Indices 6-hours prior to the cases (a) mCAPE, (b) mCIN, (d) KI and (e) TTI